

Modeling of Radio Frequency Induced Currents on Lead  
Wires During MR Imaging Using a Modified Transmission  
Line Method (MoTLiM)

A THESIS

SUBMITTED TO THE DEPARTMENT OF ELECTRICAL AND

ELECTRONICS ENGINEERING

AND THE INSTITUTE OF ENGINEERING AND SCIENCES

OF BILKENT UNIVERSITY

IN PARTIAL FULFILLMENT OF THE REQUIREMENTS

FOR THE DEGREE OF

MASTER OF SCIENCE

By

Volkan Açıkel

August 2010

I certify that I have read this thesis and that in my opinion it is fully adequate, in scope and in quality, as a thesis for the degree of Master of Science.

---

Prof. Dr. Ergin Atalar(Supervisor)

I certify that I have read this thesis and that in my opinion it is fully adequate, in scope and in quality, as a thesis for the degree of Master of Science.

---

Prof. Dr. Ayhan Altıntaş

I certify that I have read this thesis and that in my opinion it is fully adequate, in scope and in quality, as a thesis for the degree of Master of Science.

---

Prof. Dr. Nevzat G. Gencer

Approved for the Institute of Engineering and Sciences:

---

Prof. Dr. Levent Onural  
Director of Institute of Engineering and Sciences

## ABSTRACT

# Modeling of Radio Frequency Induced Currents on Lead Wires During MR Imaging Using a Modified Transmission Line Method (MoTLiM)

Volkan Açıkel

M.S. in Electrical and Electronics Engineering

Supervisor: Prof. Dr. Ergin Atalar

August 2010

Magnetic resonance imaging (MRI) is widely used diagnosis technique. During MRI radio frequency (RF) fields are utilized to excite the spins. If these RF fields incidence on metallic implants, currents will be induce on the metallic parts of implants. Inside the body these induced currents on metallic implants cause heating of tissue and sometimes cause severe burning of tissue. This phenomena makes MRI hazardous for patients with metallic implants. Much work has been done to understand this phenomena. However, most of these work based on purely experimental or numerical methods. So to understand and to obtain a good intuition on this problem a lot of cases must be solved computationally or tested experimentally.

In this study lumped element model of the transmission line is modified in order to model the conductive wires of implants inside the body. This model is based on the similarity between the damped oscillatory behavior of transmission line currents and induced currents on wires inside the body. A voltage source is added to model the effect of the incident electric field. Voltages and currents on a

infinitesimally small portion of wire are solved. Solving currents and voltages simultaneously on the modified lumped element model lead to a non-homogeneous differential equation for the current. The solution of this differential equation gives the analytical solution for the induced current on the implant lead. To test the validity of this solution, wire under the uniform incident electric field is solved with the Modified Transmission Line Method (MoTLiM) and compared to Methods of Moment (MoM) solution. The results are also verified using phantom experiments. For experimental verification, the distorted flip angle distribution due to induced currents are measured using flip angle imaging techniques. In addition to this, the flip angle distribution around the wire is calculated using results obtained from MoTLiM. Finally these results are compared and an error analysis is carried out.

*Keywords:* MRI, Implant safety, RF, Induced currents, RF Heating

## ÖZET

### Modifiye İletim Hattı Methodu Kullanılarak Radyo Frekans Dalgaları Kaynaklı Akımların Modellenmesi

Volkan Açikel

Elektrik ve Elektronik Mühendisliği Bölümü Yüksek Lisans

Tez Yöneticisi: Prof. Dr. Ergin Atalar

Ağustos 2010

Manyetik Resonans Görüntüleme (MRG) tanı koymada sık kullanılan bir tekniktir. Fakat MRG vücudunda ekite bulunan hastalar için tehlikelidir. MRG sırasında radyo frekans (RF) dalgaları spinlerin uyarılmasında kullanılmaktadır. Eğer bu RF dalgalar metal bir cisim üzerine uygulanırsa, metal cisim üzerinde akım oluşmasına neden olacaktır. Metal cisimlerde oluşan bu akımlar vücut içerisinde ciddi ısınmalara hatta bazı durumlarda dokularda ciddi yanıklara neden olabilmektedir. Bu durum MRGyi bazı hastalar için tehlikeli kılmaktadır. Bu problemi çözmek için bir çok çalışma yapılmıştır. Fakat bu çalışmalar genellikle deneysel veya benzetim tabanlı metodlarla yapılmıştır.

Bu tez çalışmasında RF dalgalar nedeniyle metaller üzerinde oluşan akımlar arasındaki ilişki analitik olarak formülize edilmiştir. Bu çözümü elde etmek için vücut içerisinde bulunan teller iletim hatları ile benzer bir biçimde modellenmiştir. Teller iletim hatlarında olduğu gibi direnç, kondansatör ve endüktans bobinleri ile modellenmişlerdir. Bu model oluşturulurken iletim hatlarında oluşan akımlar ile vücut içerisindeki teller üzerinde oluşan akımların sönümlenen salınan karakterlerinin benzerlikleri temel alınmıştır. Geleneksel iletim hattı modeli RF dalgaların etkisini dahil etmek için değiştirilmiştir. Sunulan yöntemin

geçerliliđi ilk olarak benzetimlerle test edilmiř daha sonra da deneysel yollarla dođrulanmıřtır.

*Anahtar Kelimeler:* Manyetik Rezonans Grntleme, Ekit Gvenliđi, Radyo Frekans, RF Isınma

## ACKNOWLEDGMENTS

Existence of this thesis is in virtue of many people. In the first place, I would like to express my sincere appreciation and gratitude to Prof. Ergin Atalar for his wise and scholarly comments and endless support during this thesis work. He has provided an optimum working and research environment at the UMRAM (National MR Research Center). I am also indebted to Prof. Ayhan Altıntaş and Prof. Nevzat G. Gencer for showing interest and using their precious times to read this thesis and gave their critical comments about it. The discussions and cooperations with all of my colleagues have, also, contributed substantially to this work. I am thankful to Burak Akın and Özay Hırlakoğlu because they helped me with their outstanding skills of building experimental setups. I acknowledge my gratitude to Emre Kopanoğlu because of his great patience even for answering my unintelligent, repeating questions about handling fields in time domain, lab frame, and rotating frame. I would like to thank İbrahim Mahçiçek because of his valuable comments and discussions throughout this work. It is a pleasure to pay tribute also to all members of UMRAM because of their companionship throughout the time of this study. Finally, I owe special gratitude to my parents and my sister for their continuous and unconditional support.

This work is partially supported by TUBITAK BİDEB scholarship number 2228.

# Contents

<b>1</b>	<b>INTRODUCTION</b>	<b>1</b>
<b>2</b>	<b>Modeling</b>	<b>4</b>
2.1	Transmission Line Theory . . . . .	4
2.2	Modified Transmission Line Model . . . . .	6
2.3	Solution of the Current Under Uniform Electric Field . . . . .	7
2.4	Determination of $Z$ and $k_t$ Parameters . . . . .	8
2.4.1	Bare Wire . . . . .	8
2.4.2	Lossy Bare Wire . . . . .	11
2.4.3	Insulated Wire . . . . .	12
<b>3</b>	<b>Applications and Results</b>	<b>14</b>
3.1	Bare Wire, Lossy Bare Wire Insulated Wire . . . . .	14
3.2	Wire Bisected with a Resistor . . . . .	17
3.3	Wire with Electrode . . . . .	18

3.4	Thevenin Equivalent of a Wire . . . . .	18
3.5	SAR Distribution Along a Wire . . . . .	23
<b>4</b>	<b>Experimental Verification and Experimental Results</b>	<b>25</b>
4.1	$B_1$ mapping . . . . .	28
4.2	Experimental Results . . . . .	29
<b>5</b>	<b>Discussion and Conclusion</b>	<b>33</b>

# List of Figures

1.1	The photography of a cardiac pacemaker. The lead of the pacemaker is between 50 and 60cm The photography was taken from <a href="http://en.wikipedia.org/wiki/Pacemaker">http://en.wikipedia.org/wiki/Pacemaker</a> . . . . .	1
1.2	Implants, such as pacemakers, are prohibited inside the MRI scanner. Coupling with radio frequency fields makes implants, with metallic parts, hazardous. . . . .	2
2.1	The transmission line model using lump circuit elements. . . . .	5
2.2	The modified transmission line model using lumped circuit elements that includes a series voltage source. Ground is the body with an infinite extent. . . . .	7

- 3.1 Induced current on a wire with length  $0.25m$  and radius  $0.57mm$ . (a) at  $64MHz$  and (b) at  $128MHz$  for a bare wire, (c) at  $64MHz$  and (d) at  $128MHz$  for a coated wire with coating thickness  $5\mu m$ , (e) at  $64MHz$  and (f) at  $128MHz$  for a lossy bare wire. A wire under uniform E-field exposure solved using both FEKO(EM Software & Systems Germany, Böblingen, GmbH) and MoTLiM. During simulations, wire was located inside a lossy medium with an infinite extent. The medium has  $0.42S/m$  and 81 conductivity and relative permittivity, respectively. Black solid lines are MoTLiM results and red dashed lines are FEKO results. . . . . 16
- 3.2 Induced current on a wire, bisected with a  $1k\Omega$  resistor in the middle, with length  $0.5 m$  and radius  $0.57mm$ . (a) for 1.5 tesla (b) for 3 tesla MRI scanner. A wire under uniform E field exposure solved using both FEKO and MoTLiM. During simulations wire located inside a lossy medium with infinite extent. Medium has  $0.42S/m$  and 81 conductivity and relative permittivity respectively. Black solid lines are MoTLiM results and red dashed lines are FEKO results. . . . . 19
- 3.3 Induced current on a wire with length  $0.25 m$  and radius  $0.57mm$  terminated with an electrode at one end. A spherical electrode with diameter  $4mm$  was used. (a) for 1.5 tesla (b) for 3 tesla MRI scanner. A wire under uniform E field exposure solved using both FEKO and MoTLiM. During simulations wire located inside a lossy medium with infinite extent. Medium has  $0.42S/m$  and 81 conductivity and relative permittivity respectively. Black solid lines are MoTLiM results and red dashed lines are FEKO results. 20

3.4	Thevenin Equivalent of a wire with an electrode. Wire can be represented with a Thevenin voltage source and a Thevenin impedance. Also as mentioned above electrodes can be represented with an impedance. So a wire with an electrode can be represented with this circuit. . . . .	21
3.5	Current through the electrode connected to a bare wire with 0.1 mm thickness and 0.5 m length. Spherical electrodes with 1, 2, 3 and 4 mm radii was used. (a) is for 3T MRI scanner (b) is for 1.5T MRI scanner . . . . .	22
3.6	Theoretically calculated SAR gain values near the charge, under 3T static field, for different lengths of leads in a medium with conductivity $0.4S/m$ and relative permeability of 80. . . . .	24
4.1	Wire location inside phantom. Conductivity and relative permittivity of the phantom was $0.42S/m$ and 81, respectively. Phantom was 28cm in diameter and 6.5cm high. Phantom was solution of %0.2 copper sulfate %0.1 sodium chloride %1.5 hydroxyethyl cellulose. A circulated bare copper wire with radius 0.57mm was used. The wire was located on a circle with a 12cm radius and 3.2cm above the bottom of the phantom. The phantom was located such that the center of the phantom coincided with the center of the transmit coil. . . . .	26
4.2	Flip angle images. (a) is the flip angle distribution obtained using DAM. (b) is the flip angle distribution calculated theoretically as explained in Sec. 4. $60 \times 100 \text{ mm}^2$ portion of $300 \times 65 \text{ mm}^2$ images are presented in same color scale. Flip angle values are degree. . .	30

4.3 Flip Angle distribution on a circle, centered on wire, with radius  
(a) 4 cm, (b) 6 cm, (c) 8 cm, (d) 16 cm. Flip angle values are  
degree. . . . . 31

# Chapter 1

## INTRODUCTION

Magnetic resonance imaging (MRI) is an important diagnostic imaging tool. Main advantage of MRI is its ability to obtain high soft tissue contrast and resolution. MRI is known as a very safe imaging technique, except for patients with metallic implants like pacemakers or deep brain stimulation (DBS) probes. These implants contains metallic wires and electrodes, a pacemaker can be seen in figure 1.1. These metallic wires inside the lead of implants can couple to incident radio frequency (RF) field. This coupling can cause induced currents and it can cause current flow inside the tissue. Because of this issues implants, such as pacemakers, are prohibited inside the MRI scanner.

Due to this coupling there is a high risk of serious RF heating and tissue damage due to the induced currents on leads of the implants. RF heating is

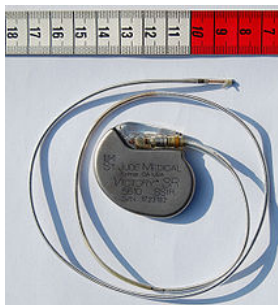


Figure 1.1: The photography of a cardiac pacemaker. The lead of the pacemaker is between 50 and 60cm The photography was taken from <http://en.wikipedia.org/wiki/Pacemaker>



Figure 1.2: Implants, such as pacemakers, are prohibited inside the MRI scanner. Coupling with radio frequency fields makes implants, with metallic parts, hazardous.

the result of altered electric field distribution where a conductive wire exists [1]. Much work has been done to understand the effect of induced currents on metallic wires inside the human body [2, 3], most of which were based on experimental studies[4] or numerical simulations[1, 5]. A solution that shows the relation between the induced current on the wires and the position of the wire in the body, the wire dimensions and insulation thickness, would help to understand the design parameters of the problem.

King has summarized an analytical formulation that was developed for center-fed insulated antennas, which was motivated by the use of insulated antennas in sea water [6]. In this approach, a dipole antenna in sea water was modeled as a transmission line with an infinite outer conductor. King showed that currents on dipole or monopole antennas have the nature of a traveling wave[7]. He states that the current on a finite dipole or monopole can be represented as a superposition of traveling waves in both directions along the antenna[7]. This traveling wave behavior is similar to transmission line currents[8]. In all these works antennas were examined inside highly conducting mediums. This kind of approach can be used to analyze induced currents on wires under an electromagnetic field inside a lossy medium. Using the assumption that scattered fields from wire will decay quickly, this approach can be used to analyze induced currents on conductive implants inside low-conductive tissues.

In this work, a novel method to analytically solve induced currents on the implant leads under MRI is found by modifying lumped element model of transmission lines. In this thesis, the modified lumped element model and the derivation of modified telegrapher's equations are presented. First, required parameters are derived to formulate the induced currents. Then for obtained analytical solution under uniform electric field exposure was compared with computer simulations for bare wire, insulated wire, lossy bare wire, and bare wire bisected with a resistor cases. Also, specific absorption rate (SAR) amplification due to the existence of a wire was calculated. After these applications a Thevenin equivalent circuit of a wire with an electrode is derived. Finally, proposed method is verified by experimentally.

# Chapter 2

## Modeling

In this study, a phasor notation with a time dependence of  $e^{i\omega t}$ , where  $\omega$  represents the angular frequency and  $i = \sqrt{-1}$ , is used. The complex wavenumber is defined as  $k = \omega\sqrt{\mu\epsilon - i\sigma/\omega}$ , and  $\epsilon$ ,  $\mu$ , and  $\sigma$  are the permittivity, permeability, and conductivity of the medium, respectively. The intrinsic impedance of the medium is defined as  $\eta = \sqrt{\mu/(\epsilon - i\sigma/\omega)}$ .

### 2.1 Transmission Line Theory

Transmission Line theory is the step between circuit theory and electromagnetic field analysis. Wave propagation along the transmission lines can be analyzed by both circuit theory and Maxwell's equations.

Transmission lines theory differs from circuit theory by electrical size of the components. In circuit theory components are much smaller than wavelength. However transmission lines are comparable with the wavelength. As the electrical size of the components became comparable with the electrical length magnitude and phase of the voltages and currents can be vary with the position on the component.

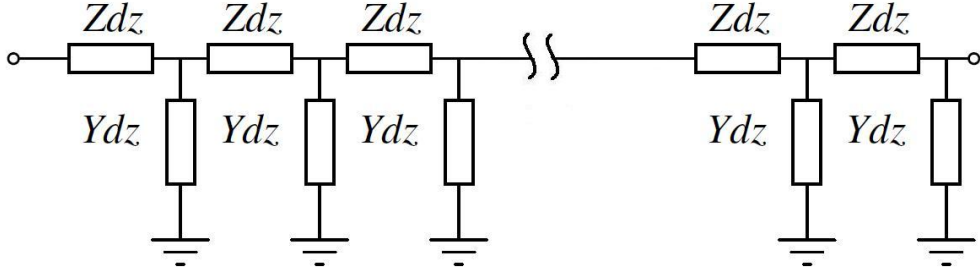


Figure 2.1: The transmission line model using lump circuit elements.

Transmission lines are usually composed of two conductors and it is modeled using series and parallel lumped elements as in Figure 2.1. where  $Z$  is the series impedance per unit length and  $Y$  is the parallel admittance per unit length as shown in Figure 2.1.

$$\begin{aligned} Z &= i\omega L + R \\ Y &= i\omega C + G \end{aligned} \quad (2.1)$$

In this model, the current on the wire,  $I$ , and voltage between the conductors of the wire are defined as a function of position  $l$ . Note that position is defined along the length of the wire. When a small portion of transmission line with length  $\delta l$  is considered voltage and current relations between points  $l$  and  $l + \delta l$  can be written as:

$$\begin{aligned} v(l, t) - R\delta l i(l, t) - L\delta l \frac{di(l, t)}{dt} - v(l + \delta l, t) &= 0 \\ i(l, t) - G\delta l v(l + \delta l, t) - C\delta l \frac{dv(l + \delta l, t)}{dt} - i(l + \delta l, t) &= 0 \end{aligned} \quad (2.2)$$

by doing some algebra and taking the limit  $\delta l \rightarrow 0$  gives the differential equations:

$$\begin{aligned} \frac{dV}{dl} &= -ZI(l) \\ \frac{dI}{dl} &= -YV(l) \end{aligned} \quad (2.3)$$

then simultaneous solution of equation 2.3 yields to solution for current:

$$I(l) = I_+ e^{-jk_t l} + I_- e^{jk_t l} \quad (2.4)$$

where  $k_t = \sqrt{-ZY}$ . Using the same theory, the characteristic impedance of the transmission line,  $Z_c$ , can be calculated as  $Z_c = \sqrt{Z/Y}$ .

Transmission line parameters can be derived in terms of electric and magnetic fields inside the transmission line. To make this derivation stored electromagnetic energy per unit length and power loss per unit length relations can be used.

## 2.2 Modified Transmission Line Model

Transmission line theory does not use a current or voltage source in its model. These sources may be used at the terminals of the transmission line in the form of boundary conditions.

In case of a wire, in a lossy medium that is exposed to an electromagnetic wave, there is only one conductor and there are no lumped source elements. Therefore, without modification, the transmission line model cannot be applied.

This problem can be solved by introducing a series voltage source and defining the shunt admittance in between the wire and the environment as shown in Figure 2.2. Also the assumption that the scattered fields decay fast must be hold so that this model can be used. The above model can be formulated using the following equation:

$$I(z) + \frac{1}{k_t^2} \frac{d^2 I(z)}{dz^2} = \frac{E^i(z)}{Z} \quad (2.5)$$

where  $E^i$  represents the tangential component of the incident electric field,  $k_t = \sqrt{-ZY}$  is the wavenumber along the wire, and  $Z$  is the distributed impedance. In this model, the wire diameter is assumed to be significantly smaller than the wavelength and therefore the electric field on the wire can be defined. The

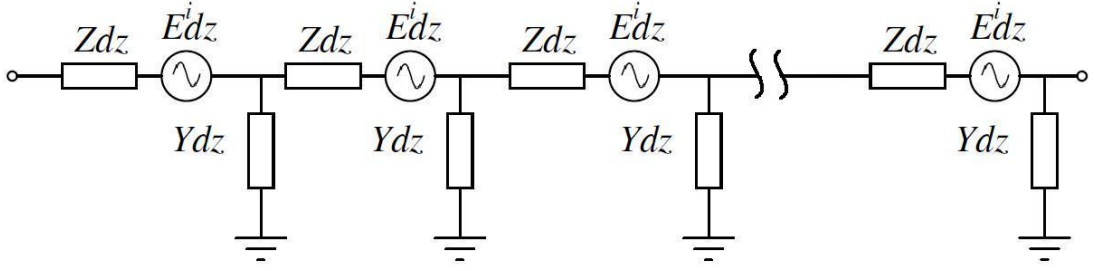


Figure 2.2: The modified transmission line model using lumped circuit elements that includes a series voltage source. Ground is the body with an infinite extent.

voltage source in Figure 2.2 models the effect of the incident field. Current along the wire can be defined and can be measured, however voltage along the wire can not be defined. To define voltage there is a need for a specific path, but in this case a path to define voltage is not exists. However defining a virtual voltage, which can not be measured, is makes easier to define boundary conditions for some cases. This virtual voltage,  $V_v(z)$  can be defined as:

$$V_v(z) = -\frac{1}{Y} \frac{dI(z)}{dz} \quad (2.6)$$

## 2.3 Solution of the Current Under Uniform Electric Field

Birdcage coils have fairly uniform E-field distribution along their main axis[9], so implants exposed to uniform E-field distribution is an important and likely situation. In this section induced currents on wires under uniform E-field are solved.

Assume a wire with length  $l$  and radius  $a$  is located on the  $z$ -axis. To find the current on the wire Eq. 2.5 must be solved. For the specific case where the

incident E-field is uniform along the wire, the solution to the Eq. 2.5 current can be found as:

$$I(z) = Ae^{-ik_t z} + Be^{ik_t z} + \frac{E}{Z} \quad (2.7)$$

where  $k_t$  and  $Z$  will be found in Section 2.4 and the unknowns  $A$  and  $B$  which will be found by the following boundary conditions:

$$\begin{aligned} I(z = l/2) &= 0 \\ I(z = -l/2) &= 0 \end{aligned} \quad (2.8)$$

applying Eq. 2.8 current on the wire can be found as:

$$I(z) = \frac{E_{z0}}{Z} - 2\frac{E_{z0}}{Z} \frac{\sin(k_t \frac{l}{2})}{\sin(k_t l)} \cos(k_t z) \quad (2.9)$$

## 2.4 Determination of $Z$ and $k_t$ Parameters

As seen in Eq. 2.9, induced current on a wire can be found if  $Z$  impedance per unit length,  $k_t$  wavenumber along the wire, and the incident E-field are known. So, a wire can be characterized by  $Z$  and  $k_t$  parameters that summarize the electrical parameters of the body and physical features of the wire. However, traditional ways of determining  $Z$  and  $k_t$  in transmission line theory is not valid for the presented case and a new approach must be used to find these parameters. In this section, the determination of  $Z$  and  $k_t$  will be shown first for a perfect conductor bare wire, then for a lossy bare wire, and finally for an insulated wire.

### 2.4.1 Bare Wire

Assume that an infinitely long perfect electrical conductor wire with a radius of "a" is placed on the  $z$ -axis and is exposed to an incident plane wave such that :

$$E_z^i = E_{z0} e^{-i\beta_z z} \quad (2.10)$$

and this plane wave can be expressed as infinite sum of cylindrical waves as [10]:

$$E_z^i = E_{z0} \sum_{n=-\infty}^{\infty} i^{-n} J_n(k_\rho \rho) e^{jn\phi} e^{-i\beta_z z} \quad (2.11)$$

where  $\rho$ ,  $\phi$  and  $z$  are the cylindrical coordinate parameters and  $J_n(\cdot)$  is  $n$ th order Bessel function. We assume  $\beta_z$  is a real parameter and  $k_\rho^2 = k^2 - \beta_z^2$ .

When the thin wire assumption holds, the term  $n = 0$  is dominant in the summation that seen in Eq. 2.11. Therefore, the incident field can be considered as [10]:

$$\begin{aligned} E_z^i &= E_{z0} J_0(k_\rho \rho) e^{-i\beta_z z} \\ H_\phi^i &= E_{z0} \frac{i}{\eta} J_1(k_\rho \rho) e^{-i\beta_z z} \end{aligned} \quad (2.12)$$

In this case, the induced current on the wire,  $I$ , will be uniform along the length of the wire. To find the relation between the incident electric field,  $E_{z0}$  and  $I$ , we need to solve electromagnetic field in the medium.

The total fields should be in the form:

$$\begin{aligned} E_z^t &= \left( A J_0(k_\rho \rho) + B H_0^{(2)}(k_\rho \rho) \right) e^{-i\beta_z z} \\ E_\rho^t &= i \frac{\beta_z}{k_\rho} \left( A J_1(k_\rho \rho) + B H_1^{(2)}(k_\rho \rho) \right) e^{-i\beta_z z} \\ H_\phi^t &= i \frac{1}{\eta} \left( A J_1(k_\rho \rho) + B H_1^{(2)}(k_\rho \rho) \right) e^{-i\beta_z z} \end{aligned} \quad (2.13)$$

$z$  and  $\rho$  components of H-field and  $\phi$  component of the E-field should be as;

$$H_z^t = 0, H_\rho^t = 0, E_\phi^t = 0$$

where A and B are the constants to be determined by boundary conditions and  $H_n^{(2)}(\cdot)$  is Hankel function of second kind.

Since scattered fields from an infinite conducting cylinder must be represented as cylindrical traveling wave functions, choosing scattered fields as a Hankel function of second kind is convenient[10]. So scattered fields are expressed as:

$$E_z^s = E_{z0} B H_0^{(2)}(k_\rho \rho) e^{-i\beta_z z} \quad (2.14)$$

Since the tangential electric field on a perfect conductor has to be zero [11] and the effect of the incident field will be dominant at the far field, the total fields can be rewritten as:

$$E_z^t = E_{z0} \left( J_0(k_\rho \rho) - \frac{J_0(k_\rho a)}{H_0^{(2)}(k_\rho a)} H_0^{(2)}(k_\rho \rho) \right) e^{-i\beta_z z} \quad (2.15)$$

$$H_\phi^t = iE_{z0} \frac{1}{\eta} \left( J_1(k_\rho \rho) - \frac{J_0(k_\rho a)}{H_0^{(2)}(k_\rho a)} H_1^{(2)}(k_\rho \rho) \right) e^{-i\beta_z z} \quad (2.16)$$

On the surface of the conductor the total tangential magnetic field is:

$$\begin{aligned} H_\phi^t(\rho = a) &= iE_{z0} \frac{1}{\eta} \left( J_1(k_\rho a) - \frac{J_0(k_\rho a)}{H_0^{(2)}(k_\rho a)} H_1^{(2)}(k_\rho a) \right) e^{-i\beta_z z} \\ &= iE_{z0} \frac{1}{\eta} \left( \frac{J_1(k_\rho a) Y_0(k_\rho a) - J_0(k_\rho a) Y_1(k_\rho a)}{H_0^{(2)}(k_\rho a)} \right) e^{-i\beta_z z} \end{aligned} \quad (2.17)$$

Applying the Wronskian of Bessel functions [12]:

$$J_n(x) Y_n'(x) - J_n'(x) Y_n(x) = \frac{2}{\pi x} \quad (2.18)$$

where ' denotes the derivative with respect to the entire argument of the Bessel function, Eq. 2.17 becomes:

$$H_\phi^t(\rho = a) = -\frac{2E_{z0}}{\eta k_\rho a \pi} \frac{1}{H_0^{(2)}(k_\rho a)} e^{-i\beta_z z} \quad (2.19)$$

the induced current on the infinite wire can be found as:

$$\begin{aligned} I &= 2\pi a H_\phi^t \\ &= -\frac{4E_{z0}}{\eta k_\rho} \frac{1}{H_0^{(2)}(k_\rho a)} e^{-i\beta_z z} \end{aligned} \quad (2.20)$$

Returning back to MoTLiM described by Eq. 2.5, the incident electric field with a linear phase variation along the length of an infinitely long wire generates a current in the same form, i.e.  $I = I_0 \exp(-i\beta_z z)$ . Therefore our differential equation turns into:

$$I_0 + \frac{\beta_z^2}{k_{t,bare}^2} I_0 = \frac{E_{z0}}{Z_{bare}} \quad (2.21)$$

To find  $Z$  and  $k_t$  Eq. 2.20 is used in Eq. 2.21 and assumed that field variation along the wire is small,  $\beta_z < |k|$ , and then  $H_0^{(2)}(k_\rho a) \approx H_0^{(2)}(ka)$ . The effect of this assumption on the accuracy of the model will be discussed later. Then with some manipulations  $Z$  and  $k_t$  can be obtained as:

$$Z_{bare} = \frac{\eta k}{4} H_0^{(2)}(ka) \quad (2.22)$$

$$k_{t,bare} = k \quad (2.23)$$

## 2.4.2 Lossy Bare Wire

In the previous section, analysis of a perfect electrical conductor wire was performed. Now assume that the wire has a finite conductivity  $\sigma_c$ .

As known from transmission line theory,  $Z$ , impedance per unit length, includes loss of the conductor. So  $Z$  and  $k_t = \sqrt{-ZY}$  must be redefined. For a lossy wire impedance per unit length in the lumped element model could be defined as:

$$Z_{lossy} = Z_{bare} + Z_{wire} \quad (2.24)$$

where  $Z_{lossy}$  is impedance per unit length for lossy wire,  $Z_{bare}$  is impedance per unit length for a perfect conductor and  $Z_{wire}$  is impedance due to the loss of the

conductor and can be expressed as:

$$Z_{wire} = \frac{1}{2\pi a \delta_c \sigma_c} \quad (2.25)$$

where  $\delta_c$  is the skin depth and defined as [8]:

$$\delta_c = \frac{1}{\sqrt{\pi f \mu \sigma_c}} \quad (2.26)$$

As  $Z_{lossy}$  is known,  $k_{t,lossy}$  can be defined as:

$$k_{t,lossy} = k_{t,bare} \sqrt{1 + \frac{Z_{wire}}{Z_{bare}}} \quad (2.27)$$

### 2.4.3 Insulated Wire

To analyze insulated wires,  $Z$  and  $k_t$  must be recalculated as in the previous section. To do this fields and boundary conditions, which were stated in the previous section, must be redefined. As a dielectric material on the conductor exists, there must be two boundaries; one between the tissue and the dielectric material, at  $\rho = b$ , and one between the dielectric and the conductor  $\rho = a$ . Parameters with superscript  $d$  are parameters of the insulator. Total fields inside the dielectric are:

$$\begin{aligned} E_{zd}^t &= A^d J_0(k_\rho^d \rho) + B^d H_0^{(2)}(k_\rho^d \rho) \\ H_{\phi d}^t &= \frac{i}{\eta_d} \left( A^d J_1(k_\rho^d \rho) + B^d H_1^{(2)}(k_\rho^d \rho) \right) \end{aligned} \quad (2.28)$$

and total fields inside the tissue are:

$$\begin{aligned} E_z^t &= A J_0(k_\rho \rho) + B H_0^{(2)}(k_\rho \rho) \\ H_\phi^t &= \frac{i}{\eta} \left( A J_1(k_\rho \rho) + B H_1^{(2)}(k_\rho \rho) \right) \end{aligned} \quad (2.29)$$

boundary conditions can be defined as:

$$E_{zd}^t(\rho = a) = 0 \quad (2.30)$$

$$E_{zd}^t(\rho = b) = E_z^t(\rho = b)$$

$$H_{\phi d}^t(\rho = b) = H_\phi^t(\rho = b)$$

$$H_{\phi d}^t(\rho = a) = J_s \quad (2.31)$$

where  $J_s$  is surface current density and can be expressed as:  $J_s = I/2\pi a$

applying boundary conditions current on infinitely long insulated wire can be found as:

$$I = -E_{z0} \frac{4}{\eta k_\rho} \frac{1}{H_0^{(2)}(k_\rho b) + k_\rho^d b \log(\frac{b}{a}) H_1^{(2)}(k_\rho b)} \quad (2.32)$$

When an infinitesimally small portion of wire is considered, insulation can be thought as a capacitor series to the  $Y$  in the lumped element model. Thus when insulating a wire only  $Y$  will change.  $Z$  will remain as in Eq. 2.22, for a wire with radius  $b$ .

$$Z_{bare} = \frac{\eta k}{4} H_0^{(2)}(kb) \quad (2.33)$$

Then using Eq. 2.32 in Eq. 2.21 the propagation constant along the wire can be written as:

$$k_{t,insulated} = \sqrt{-\frac{\eta k_\rho \beta_z^2 H_0^{(2)}(k_\rho b)}{k_\rho^d b \log(\frac{b}{a}) H_1^{(2)}(k_\rho b)}} \quad (2.34)$$

# Chapter 3

## Applications and Results

In this chapter validity of MoTLiM tested. Several cases are solved with MoTLiM and compared to FEKO simulations. In this Chapter all simulations done inside a homogeneous medium with conductivity 0.42 S/m, relative permittivity 81 under uniform E-field exposure for 1.5 and 3 Tesla MRI scanners. During all analysis a wire, with length  $l$  and radius  $a$ , assumed to be located on the  $z$ -axis

### 3.1 Bare Wire, Lossy Bare Wire Insulated Wire

To find the current on the wire Equation 2.5 must be solved and by solving Equation 2.5 current can be found as:

$$I(z) = Ae^{-jkz} + Be^{jkz} + \frac{E}{Z} \quad (3.1)$$

where A and B the unknowns which will be found by applying boundary conditions:

$$\begin{aligned} I(z = l/2) &= 0 \\ I(z = -l/2) &= 0 \end{aligned} \quad (3.2)$$

applying Equation 3.2  $A$  and  $B$  can be found as:

$$A = B = -\frac{E_{z0}}{Z} \frac{\sin(k\frac{l}{2})}{\sin(kl)} \quad (3.3)$$

finally current on the wire is:

$$I(z) = -2\frac{E_{z0}}{Z} \frac{\sin(k\frac{l}{2})}{\sin(kl)} \cos(kz) + \frac{E_{z0}}{Z} \quad (3.4)$$

For the case under uniform electric field exposure, induced currents are solved using MoTLiM for bare, coated, and lossy wire cases. These solutions are compared with electromagnetic field simulations carried out using FEKO simulations. During simulations a homogeneous body with an infinite extent was used. Relative permittivity and conductivity of the body was 81 and  $0.42S/m$ , respectively. A bare perfect conductor wire with radius  $0.57mm$  and length  $0.25m$  was located on the  $z$ -axis inside the uniform body with infinite extent. Both ends of the wire were floating inside the body. A plane wave excitation, with the E-field component in  $z$ -direction, was applied so that the wire was exposed to an uniform electric field. Impedance of the bare wire was  $Z_{bare} = 193 + i670\Omega/m$  and wavenumber of wire was  $k_{t,bare} = 24.7 - i8.3m^{-1}$  for  $3T$  scanner. At  $1.5T$  impedance was  $Z_{bare} = 87.3 + i386\Omega/m$  and wavenumber of wire was  $k_{t,bare} = 14.2 - i7.5m^{-1}$ . Mean-square errors were 8% and 6% for  $3T$  (Fig. 3.1(a)) and  $1.5T$  (Fig. 3.1(b)) scanners, respectively. When a coated wire with  $5\mu m$  coating thickness and the coating of a 4 relative permittivity was replaced, impedance of wire was  $Z_{insulated} = 193 + i687\Omega/m$  and wavenumber of wire was  $k_{t,insulated} = 26.2 - i9.6m^{-1}$  for  $3T$  scanner and impedance was  $Z_{insulated} = 87.3 + i386\Omega/m$  and wavenumber of wire was  $k_{t,insulated} = 15.4 - i9.5m^{-1}$  for  $1.5T$  scanner. Mean square errors for this case was 4% and 7% for  $3T$  (Fig. 3.1(c)) and  $1.5T$  (Fig. 3.1(d)) scanners, respectively. Finally for the lossy bare wire case impedance was  $Z_{lossy} = 293 + i670\Omega/m$  and wavenumber of wire was  $k_{t,lossy} = 24.6 - i10.1m^{-1}$  for  $3T$  scanner. At  $1.5T$  impedance was  $Z_{lossy} = 187.3 + i386\Omega/m$  and wavenumber of wire was

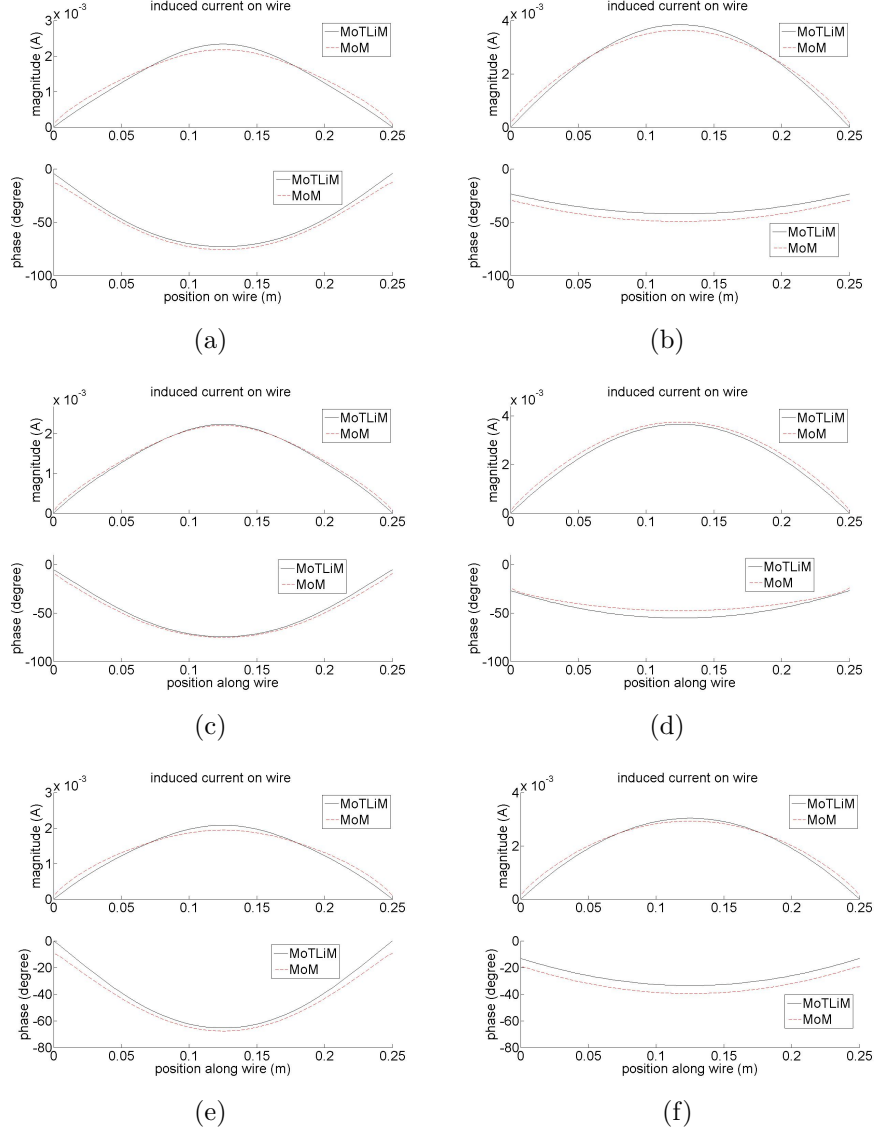


Figure 3.1: Induced current on a wire with length  $0.25m$  and radius  $0.57mm$ . (a) at  $64MHz$  and (b) at  $128MHz$  for a bare wire, (c) at  $64MHz$  and (d) at  $128MHz$  for a coated wire with coating thickness  $5\mu m$ , (e) at  $64MHz$  and (f) at  $128MHz$  for a lossy bare wire. A wire under uniform E-field exposure solved using both FEKO(EM Software & Systems Germany, Böblingen, GmbH) and MoTLiM. During simulations, wire was located inside a lossy medium with an infinite extent. The medium has  $0.42S/m$  and 81 conductivity and relative permittivity, respectively. Black solid lines are MoTLiM results and red dashed lines are FEKO results.

$k_{t,lossy} = 13.8 - i9.4m^{-1}$ . Mean-square errors were 8% and 6% for 3T (Fig. 3.1(e)) and 1.5T (Fig. 3.1(f)) scanners, respectively.

Then experimental verification of MoTLiM was done using flip angle images which were obtained both experimentally and theoretically. During experiments, a cylindrical phantom 28cm in diameter and 6.5cm high was used. Experiments were made for a bare wire to prove the validity of MoTLiM. Conductivity and relative permittivity of the phantom was 0.42S/m and 81, respectively. Electrical parameters of the phantom were measured using a custom-made transmission line probe[20] with an Agilent E5061A ENA series network analyzer. Experiments were done with a 3T Siemens TimTRIO system. A SE with TR 1000 ms TE 15 ms FOV  $300 \times 65 \text{ mm}^2$  was used. A bare copper wire with radius 0.57mm was used. Wire was circulated to form a full circle and located on a circle with 12cm radius. The wire was located 2.5cm from the bottom of the phantom. This configuration ensures that the wire was exposed to a uniform electric field. Flip angle distributions were measured and calculated. Error analysis was done along the circles, with different radii( 4 to 16cm ) around the wire. Mean-square errors are between 16% and 20%.

## 3.2 Wire Bisected with a Resistor

To solve the induced currents on wire bisected with a resistor Equation 3.1 still holds for the both sections of wire. However  $A$  and  $B$  must be determined for both sections. Boundary conditions stated in Equation 3.2 still holds but new boundary condition must be defined at the location of the resistor,  $z = 0$ , as;

$$\begin{aligned} I(z = 0^-) &= I(z = 0^+) \\ V(z = 0^-) - V(z = 0^+) &= I(z = 0)R \end{aligned} \tag{3.5}$$

Under uniform e-field voltage along the wire can be found, by using Equation 2.6, as:

$$V(z) = \frac{-ik_t}{-Y} A e^{-ik_t z} + \frac{ik_t}{-Y} B e^{ik_t z} \quad (3.6)$$

### 3.3 Wire with Electrode

Equation 3.1 is also valid for the wire terminated with an electrode. However, boundary conditions for both end of the wire must be determined and using these boundary conditions coefficients  $A$  and  $B$  must be redefined. At the open end of the wire current will still be zero and can be written as;

$$I(z = 0) = 0 \quad (3.7)$$

At the other end, terminated with electrode, of the wire current will not be zero and can be defined as;

$$\frac{V(z = l)}{I(z = l)} = Z_e \quad (3.8)$$

where  $Z_e$  is the electrode impedance and defines the properties of the electrode. Halise Irak in her thesis work defines electrode impedance[13] for a spherical electrode as;

$$Z_e = \frac{1}{2\pi\tilde{\sigma}D} \quad (3.9)$$

where  $\tilde{\sigma}$  is the complex conductivity of the medium and  $D$  is the diameter of the electrode. mean square error was 9% and 12% for 1.5T and 3T MRI scanners respectively.

### 3.4 Thevenin Equivalent of a Wire

As electrodes can be represented with a impedance, wires can be represented with a Thevenin equivalent circuit. By this way current through the electrode can be

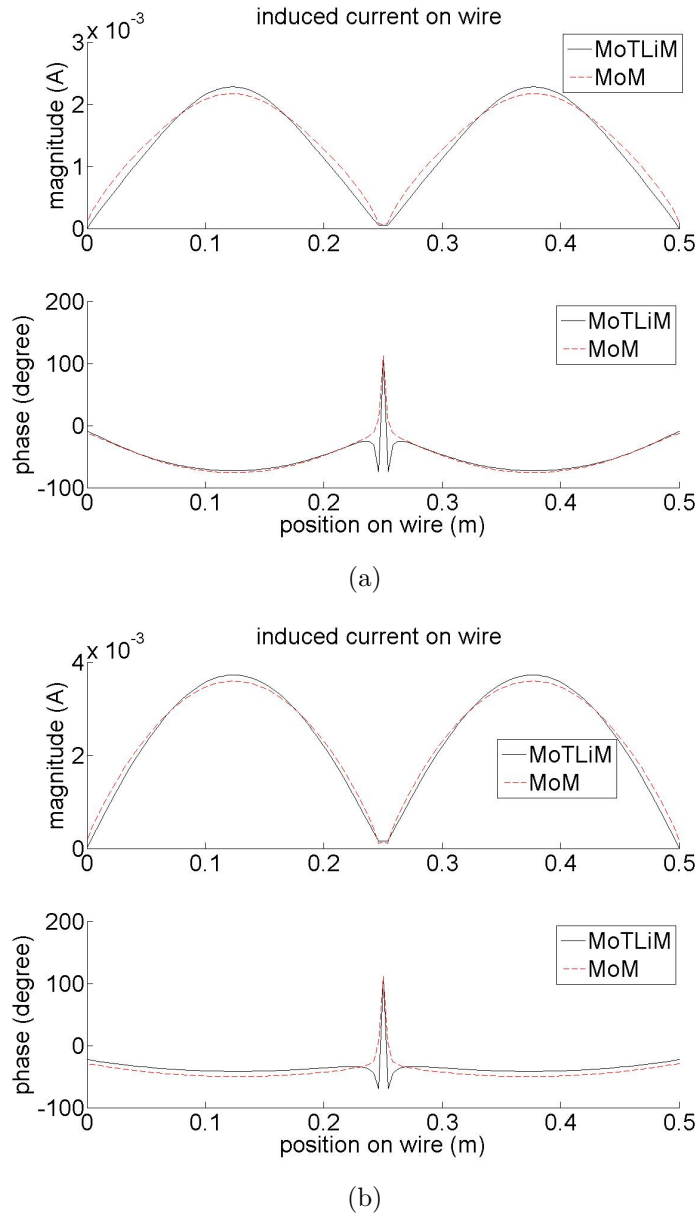
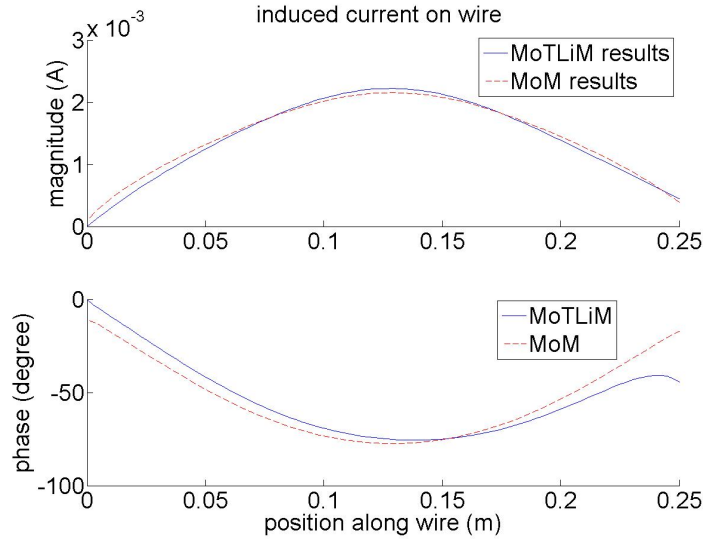
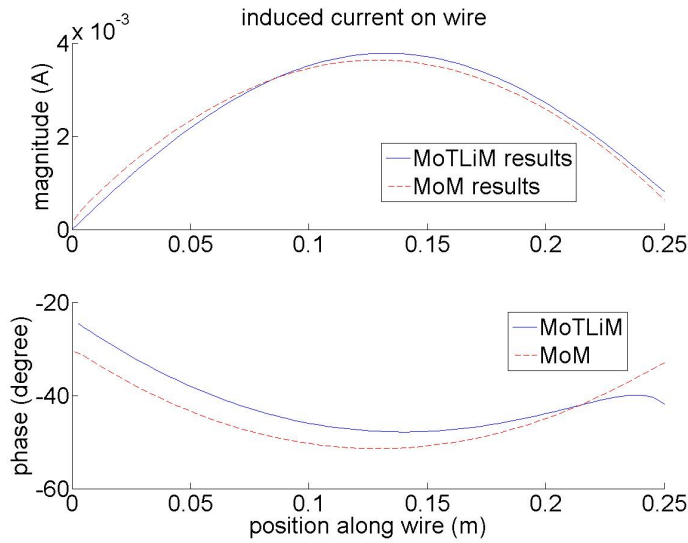


Figure 3.2: Induced current on a wire, bisected with a  $1k\Omega$  resistor in the middle, with length 0.5 m and radius 0.57mm. (a) for 1.5 tesla (b) for 3 tesla MRI scanner. A wire under uniform E field exposure solved using both FEKO and MoTLiM. During simulations wire located inside a lossy medium with infinite extent. Medium has  $0.42S/m$  and 81 conductivity and relative permittivity respectively. Black solid lines are MoTLiM results and red dashed lines are FEKO results.



(a)



(b)

Figure 3.3: Induced current on a wire with length 0.25 m and radius 0.57mm terminated with an electrode at one end. A spherical electrode with diameter 4mm was used. (a) for 1.5 tesla (b) for 3 tesla MRI scanner. A wire under uniform E field exposure solved using both FEKO and MoTLiM. During simulations wire located inside a lossy medium with infinite extent. Medium has 0.42S/m and 81 conductivity and relative permittivity respectively. Black solid lines are MoTLiM results and red dashed lines are FEKO results.

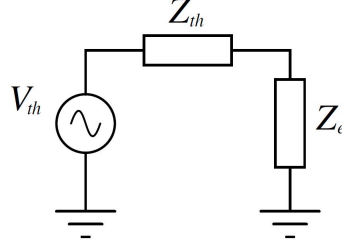


Figure 3.4: Thevenin Equivalent of a wire with an electrode. Wire can be represented with a Thevenin voltage source and a Thevenin impedance. Also as mentioned above electrodes can be represented with an impedance. So a wire with an electrode can be represented with this circuit.

found easily. In this section Thevenin equivalent of a wire will be obtained. One end of the wire will be considered to be not connected to anywhere. to find the  $V_{th}$  open circuit voltage,  $V_{open}$  at the end of the wire must be calculated. Unknown coefficients must be determined using boundary conditions. For the case of open circuit current will be zero at both ends and boundary conditions can be defined as:

$$\begin{aligned} I(z = 0) &= 0 \\ I(z = l) &= 0 \end{aligned} \quad (3.10)$$

Then to find  $Z_{th}$  short circuit current,  $I_{short}$ , must be found. Also for the short circuit current case unknown coefficients must be found again via boundary conditions. For this case boundary conditions can be determined as;

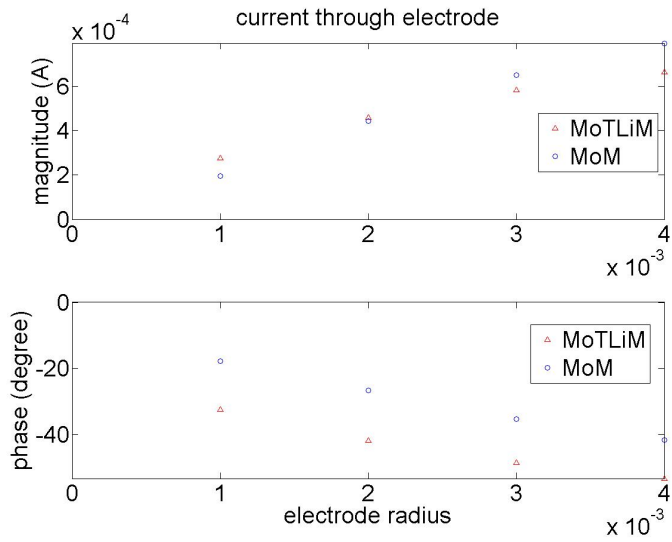
$$\begin{aligned} I(z = 0) &= 0 \\ V(z = l) &= 0 \end{aligned} \quad (3.11)$$

As open circuit voltage and short circuit current is known Thevenin impedance can be written as;

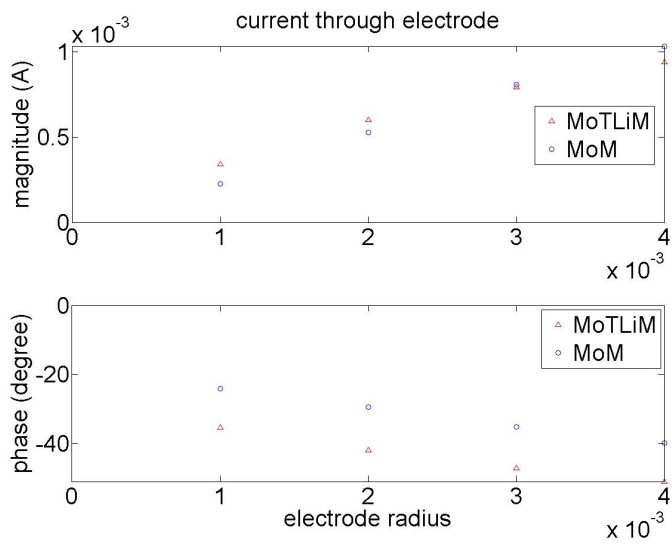
$$Z_{th} = \frac{V_{open}}{I_{short}} \quad (3.12)$$

As  $Z_{th}$ ,  $V_{th}$  and  $Z_e$  is known current through the electrode can be written as;

$$I_e = \frac{V_{th}}{Z_{th} + Z_e} \quad (3.13)$$



(a)



(b)

Figure 3.5: Current through the electrode connected to a bare wire with 0.1 mm thickness and 0.5 m length. Spherical electrodes with 1, 2, 3 and 4 mm radii was used. (a) is for 3T MRI scanner (b) is for 1.5T MRI scanner

### 3.5 SAR Distribution Along a Wire

During an MRI scan metallic implants cause severe heating around its tip [1]. This heating is a result of amplification of E-field along the conductive lead of implant. Heating of the tissue can be calculated using SAR gain distribution and Bioheat Transfer [1]. SAR gain can be calculated as:

$$Gain_{SAR} = \frac{SAR_t}{SAR_i} \quad (3.14)$$

where  $SAR_t$  is the SAR distribution in the presence of a wire and  $SAR_i$  is the SAR distribution due to incident RF field. To find the SAR distribution E-field must be known as it is known SAR can be calculated as:

$$SAR = \frac{\sigma E^2}{\rho_t} \quad (3.15)$$

where  $E$  is the magnitude of the electric field  $\sigma$  is the conductivity of the medium,  $\rho_t$  is the mass density of the tissue.

Finding current distribution along the wire is easy with MoTLiM. As current distribution is known charge distribution along the wire can be found with continuity equation:

$$\nabla \cdot J = -\frac{\partial \rho}{\partial t} \quad (3.16)$$

Then using quasi-static assumption e-field can be found along the wire so the SAR distribution can be calculated. To find the e-field point charges can be assumed on the segments along the wire. Then summing up the e-field due to these point charges e-field can be calculated.

$$E(R) = \sum_i \frac{q_i}{4\pi\epsilon_c R^2} \quad (3.17)$$

SAR distribution for different lengths of wire can be seen in Figure 3.6 for a bare wire inside a phantom with infinite extent. Wire has radius of  $0.65mm$  and calculations done for lengths of 4, 8, 12, and  $16cm$ . SAR values in Figure 3.6 was calculated just near the charges.

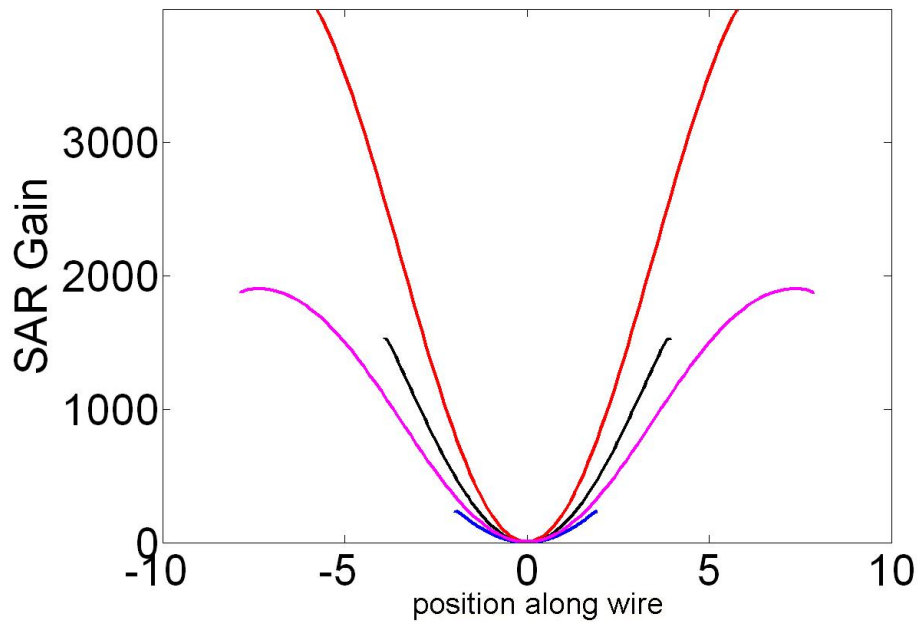


Figure 3.6: Theoretically calculated SAR gain values near the charge, under 3T static field, for different lengths of leads in a medium with conductivity  $0.4S/m$  and relative permeability of 80.

## Chapter 4

# Experimental Verification and Experimental Results

During MRI RF fields cause induced currents on metallic implants. These currents change the RF field pattern, which leads to distortion of the flip angle distribution around the metallic implants [14]. In this study, flip angle distortion due to RF-induced currents were used for verification of MoTLiM. Flip angle distribution around a copper wire was calculated theoretically and measured using flip angle imaging techniques experimentally. Then these two solutions were compared and error analysis was done.

In order to calculate the flip angle distortion caused by RF-induced currents first incident magnetic field found. During experiments a body birdcage coil were used and assumed to be ideal. So incident magnetic field can be calculated using flip angle imaging techniques[15, 16, 17]. As incident magnetic field is known incident electric field can be calculated using maxwell's equations. Then incident electric field was used in MoTLiM to calculate the induced currents on the wire. Using the results obtained from MoTLiM  $B^w$ , the magnetic field due to induced currents, was calculated. Then, the incident field and the forward polarized part

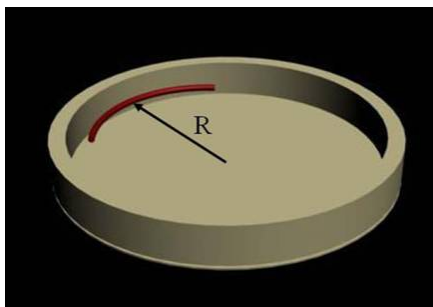


Figure 4.1: Wire location inside phantom. Conductivity and relative permittivity of the phantom was  $0.42S/m$  and  $81$ , respectively. Phantom was  $28cm$  in diameter and  $6.5cm$  high. Phantom was solution of  $\%0.2$  copper sulfate  $\%0.1$  sodium chloride  $\%1.5$  hydroxyethyl cellulose. A circulated bare copper wire with radius  $0.57mm$  was used. The wire was located on a circle with a  $12cm$  radius and  $3.2cm$  above the bottom of the phantom. The phantom was located such that the center of the phantom coincided with the center of the transmit coil.

of  $B^w$  was summed by vector summation. The obtained  $B_1$ , the total forward polarized field was used for calculating flip angle, and thus a theoretical flip angle distribution was obtained. Flip angle distribution was also obtained using flip angle imaging with distorted images. Then the flip angle image around the wire was compared with the theoretically calculated flip angle distribution around the wire and an error analysis was carried out.

For simplicity, a cylindrical phantom was placed inside the MR scanner, as seen in Figure 4.1. This geometry ensures that the incident E-field along the wire will be uniform.

A body birdcage coil was used as the transmit coil. The incident magnetic field could be approximated as:

$$B_{1f}^c \approx B_1(\cos(\omega t)\hat{x} - \sin(\omega t)\hat{y}) \quad (4.1)$$

Note that until this point phasor notation has been used. However, to find the total magnetic field in the rotating frame, fields will be written in time domain, and then in rotating frame to find the magnitude of the field that will excite the spins.

For this specific configuration only the  $y$  component of the incident magnetic field causes flux on the surface encircled by the wire. Therefore, the relation between the incident electric field and the magnetic field can be determined via Faraday's Law of Electromagnetic Induction, Eq. 4.2.

$$\oint_c E_\phi \cdot dl = - \int_s \frac{dB_y}{dt} \cdot ds \quad (4.2)$$

Assuming the incident magnetic field is uniform, and carrying out some simple algebra and using the  $y$  component of the incident magnetic field, the incident electric field along the wire can be approximated as in Eq. 4.3.

$$E_i \approx \omega \rho \frac{B_y}{2} \cos(\omega t) \quad (4.3)$$

where  $\rho$  is the radius of the circle where the wire was located. As the incident E-field is known, induced currents can be calculated using MoTLiM. Then, using quasi-static assumption, the magnetic field caused by induced currents can be found as:

$$B^w \approx \frac{\mu I(z) \cos(\omega t - \theta^w)}{2\pi r} \quad (4.4)$$

where  $\theta^w$  is the phase of the current. The magnetic field due to the induced current is a linearly polarized field, which can be written as the summation of forward polarized and backward polarized fields, as in Eq. 4.5 in cartesian coordinates. The vector summation of  $B_1$  and the forward polarized part of  $B^w$  will determine the flip angle around the wire.

$$\begin{aligned} B^w = & \frac{-|B^w| \sin(\theta)}{2} (\cos(\omega t - \theta^w) \hat{x} - \sin(\omega t - \theta^w) \hat{y}) \\ & - \frac{|B^w| \sin(\theta)}{2} (\cos(\omega t - \theta^w) \hat{x} + \sin(\omega t - \theta^w) \hat{y}) \\ & + \frac{|B^w| \cos(\theta)}{2} (\cos(\omega t - \theta^w) \hat{y} + \sin(\omega t - \theta^w) \hat{x}) \\ & + \frac{|B^w| \cos(\theta)}{2} (\cos(\omega t - \theta^w) \hat{y} - \sin(\omega t - \theta^w) \hat{x}) \end{aligned} \quad (4.5)$$

The forward polarized field due to induced currents on the wire can be written as:

$$B_f^w = \frac{-|B^w|\sin(\theta)}{2}(\cos(\omega t - \theta^w)\hat{x} - \sin(\omega t - \theta^w)\hat{y}) + \frac{|B^w|\cos(\theta)}{2}(\cos(\omega t - \theta^w)\hat{y} + \sin(\omega t - \theta^w)\hat{x}) \quad (4.6)$$

where  $\theta$  is the azimuthal angle. So, the total forward polarized field will be the vectorial summation of two forward polarized fields:

$$B_{total} = B_f^w + B_{1f}^c \quad (4.7)$$

Summing these fields in rotating frame yields a field with magnitude:

$$|B_{total}| = \sqrt{|B_1|^2 + \frac{|B^w|^2}{4} - |B_1||B^w|\sin(\theta^w + \theta)} \quad (4.8)$$

Finally, to calculate the total forward polarized magnetic field in the presence of a wire, the incident magnetic field  $B_1$  must be known.

## 4.1 $B_1$ mapping

Incident magnetic field can be measured by using flip angle imaging methods[15, 16, 17]. In this study flip angle imaging done with Spin Echo (SE) images. In order to calculate the incident magnetic field Spin Echo (se) images with several nominal voltages applied to coil, was acquired. Image intensity of SE images can be expressed as [18]:

$$S = M(x, y, z)\sin^3(\alpha(x, y, z)) \quad (4.9)$$

where  $\alpha(x, y, z)$  is the flip angle distribution and  $M(x, y, z)$  is the magnetization moment inside the phantom. Flip angle distribution calculated using Double Angle Method[17]. Flip angle distributions first calculated for phantom without placing the wire. This results are used for calculation of incident fields. Then

flip angle distributions calculated for the case which wire is located inside the phantom.

SE images which are acquired with several nominal voltages fitted to Equation 4.9. Also it is known that relation between flip angle and  $B_1$  field is [19]:

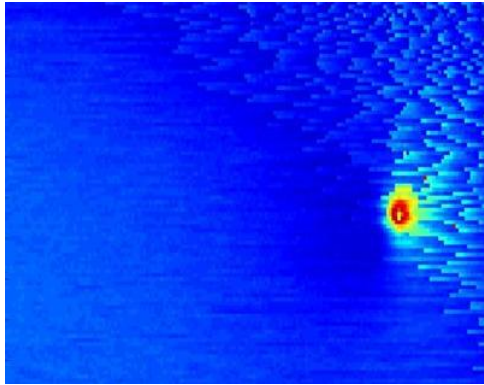
$$\alpha = 2\pi \int \gamma B_1 dt \quad (4.10)$$

where  $\gamma$  is the gyromagnetic ratio of proton. So, using fitted  $\alpha$  to Equation 4.9 and using in Equation 4.10  $B_1$  field distribution can be obtained. Also flip angle distribution in the presence of a wire can be found using curve fitting method.

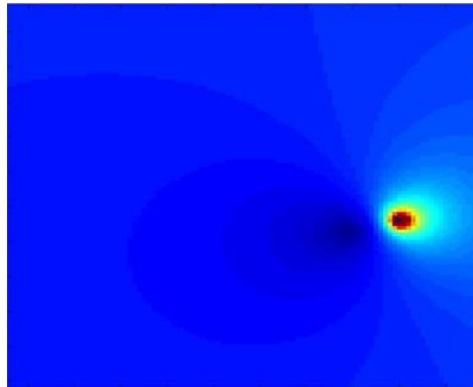
## 4.2 Experimental Results

To verify the proposed method as mentioned MoTLiM also tested experimentally by measuring and calculating flip angle distribution due to induced currents.

During experiments, a cylindrical phantom 28cm in diameter and 6.5cm high was used. Experiments were done for a bare wire to prove the validity of MoTLiM. Conductivity and relative permittivity of the phantom was 0.42S/m and 81, respectively. Electrical parameters of the phantom were measured using a custom-made transmission line probe[20] with an Agilent E5061A ENA series network analyzer. Experiments were done with a 3T Siemens TimTRIO system. A SE with TR 1000 ms TE 15 ms FOV  $300 \times 65 \text{ mm}^2$  was used. A bare copper wire with radius 0.57mm was used. Wire was circulated to form a full circle and located on a circle with 12cm radius. The wire was located 2.5cm from the bottom of the phantom. This configuration ensures that the wire exposed to a uniform electric field. Flip angle distributions were measured and calculated.



(a)



(b)

Figure 4.2: Flip angle images. (a) is the flip angle distribution obtained using DAM. (b) is the flip angle distribution calculated theoretically as explained in Sec. 4.  $60 \times 100 \text{ mm}^2$  portion of  $300 \times 65 \text{ mm}^2$  images are presented in same color scale. Flip angle values are degree.

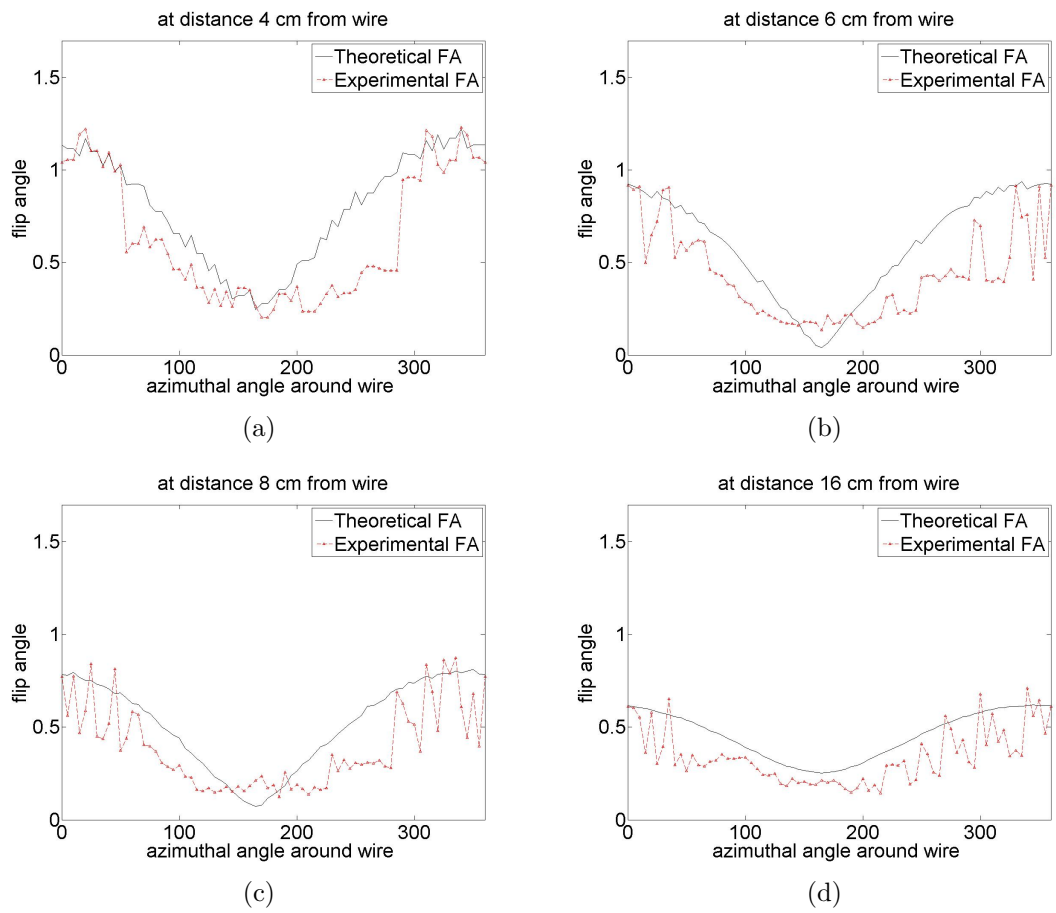


Figure 4.3: Flip Angle distribution on a circle, centered on wire, with radius (a) 4 cm, (b) 6 cm, (c) 8 cm, (d) 16 cm. Flip angle values are degree.

Error analysis was done along the circles, with different radii(4, 6, 8 and 16 $cm$ ) around the wire. Mean-square errors are 16%, 20%, 19%, and 18% for figures 4.3(a), 4.3(b), 4.3(c), and 4.3(d), respectively.

# Chapter 5

## Discussion and Conclusion

In this study a new method was proposed to solve induced currents inside a lossy medium. To show the validity of this method some simple cases (straight bare, lossy, and insulated) were solved and compared with computer simulations that uses method of moments. The analysis revealed less than 10% mean-squared error. As analyzed in Sec. 2.4, to find the required parameters wires were assumed to be infinite and induced currents were reached to a steady state. During the simulations, however, wires had a finite length. As a result, the wires were not long enough to reach steady state and thus most of the error was coming from these transition regions.

As seen from Figure 4.3, experimental and theoretical flip angle results are in good agreement. Mean-square error is less than 20%. However, there are problems with comparing measured flip angles and theoretically calculated flip angles. In vicinity of the wire, the magnetic field rapidly changes inside a pixel; while theoretically calculated flip angle for a pixel, a fixed distance inside the pixel was used. The effect of the change of magnetic field inside the pixel can not be taken into account.

Although in this study only straight bare, lossy, and insulated wires were solved, this method can be expanded to more complicated cases. As long as the tangential component of the incident electric field is known, induced currents along the wires which are located in an arbitrary pattern can be found by solving Eq. 2.5. However, scattered fields from the wire must decay fast enough so that they will not induce current on other parts of the wire. To handle this case, the modified lumped element model in Figure 2.2 must be further modified. Additionally in all solved cases in this study, wires are inside the uniform lossy medium; it is however possible to encounter a case where the wire is located inside more than one medium. This problem can be handled by considering the wires as connected transmission lines and defining boundary conditions between the transmission lines appropriately. Furthermore, using solutions obtained from the proposed theory, SAR Gain and implant tip heating can be calculated.

Using this method cases, that will cause maximum induced current, can be found so lead designs can be tested for worst cases. The newly defined  $k_t$  parameter enable to find length of the lead in terms of wavelength so resonant length of lead after modifications like coating or pitching can be found. Beside these cases of testing implant leads this method also useful for designing new leads. Effects of modifications on leads such as coiling, or adding lumped elements can be easily seen using this method. Also adjusting the  $Z$  and  $k_t$  parameters amount of induced current and pattern of the current on a lead can be adjusted. Also, presented method makes it easy to understand how newly designs, like billabong [21], works. Besides all experimental results that shows these leads are safe, presented work can show why these leads are safe.

MoTLiM can also be used for solving similar problems, such as interaction between implants and cell phones. There are works that analyze SAR gain in the presence of orthopedical and dentistry implants during the use of the cell

phones[22]. MoTLiM may also be used to calculate induced currents on these implants when they interact with the cell phones.

To sum up, a new method to calculate the induced currents on wires under MRI was demonstrated. A lumped element model of transmission lines are modified in order to find an analytical solution for induced currents on implant leads.  $Z$  and  $k_t$  parameters, which can characterize wires, are derived. Proposed method compared with MoM simulations and results are agreed within 10% mean-square error in current. A thevenin model was derived in order to find the current through the electrodes easily. Finally proposed method was verified by using image distortion due to the existence of the wire. Flip angle distribution is compared on the azimuthal paths with four different distances from the wire. The highest mean square error is 20% among compared cases.

# Bibliography

- [1] C.J.Yeung , R.C.Susil, E.Atalar "RF Safety of Wires in Interventional MRI:Using a Safety Index", Mag. Reson. Med. 47, 187–193 (2002).
- [2] M.K.Konings, L.W.Bartels, H.F.M.Smits, C.J.G. Bakker "Heating around intravascular guidewires by resonating RF waves", J. Magn. Reson. Imaging 12, 79–85 (2000).
- [3] F.G.Shellock "Radiofrequency Energy-Induced Heating During MR Procedures: A Review" J. Magn. Reson. Imaging 12, 30–36 (2000).
- [4] P.A.Bottomley, W.A.Edelstein, A.Kumar, M.J.Allen, P.Karmarkar "Resistance and Inductance Based MRI-Safe Implantable Lead Strategies". 17<sup>th</sup> Annual ISMRM Meeting, Honolulu, Hawaii, April 18-24, (2009).
- [5] C.J.Yeung , P.Karmarkar, R.M.Elliot, "Minimizing RF Heating of Conducting Wires in MRI", Mag. Reson. Med.58, 1028-1034 (2007)
- [6] R.W.P.King "The Many Faces of the Insulated Antenna" Proceedings of IEEE 64-2, 228-238 (1976).
- [7] L.C.Shen, T.T.Wu, R.W.P.King "A Simple Formula of Current in Dipole Antennas" IEEE Trans. Antennas and Propagation 16-5, 542-547 (1968)
- [8] D.M.Pozar, "Microwave Engineering", 3<sup>rd</sup> Edition, John Wiley & Sons, (2005)

- [9] J.Jianming, "Electromagnetic Analysis and Design in Magnetic Resonance Imaging" CRC Press, (1998)
- [10] C.A.Balanis. "Advanced Electromagnetics" John Wiley & Sons 1989
- [11] D.K.Cheng "Fundamentals of Engineering Electromagnetics" Pearson Addison Wesley, (1993).
- [12] G.N.Watson, "A Treatise on the Theory of Bessel Functions" Cambridge University Press
- [13] H.Irak, "Modeling RF Heating of Active Implantable Medical Devices During MRI Using Safety Index ", August (2007)
- [14] H. Graf, U.A. Lauer, A. Berger, and F. Schick, "RF artifacts caused by metallic implants or structures which get more prominent at 3 T: an in vitro study," *Magn. Reson. Imaging* 23, 493-499 (2005).
- [15] V.L.Yarnykh "Actual Flip-Angle Imaging in the Pulsed Steady: A Method for Rapid Three-Dimensional Mapping of the Transmitted Radiofrequency Field", *Mag. Reson. Med.* 57, 192-200 (2007)
- [16] E.K.Insko, L.Bolinger "Mapping of the Radiofrequency Field" *J. Magn. Reson.* 103, 82-85 (1993)
- [17] J.P.Hornak, J.Szumowski, R.G.Bryant "Magnetic Field Mapping" *Mag. Reson. Med* 6, 158-163 (1988)
- [18] G. H. Glover, C.E. Hayes, N.J.Pelc, W.A.Edelstein, O.M.Mueller, H.R. Hart, C.J. Hardy, M.O'Donnell and W.D.Barber, "Comparison of Linear and Circular Polarization for Magnetic Resonance Imaging" *J. Magn. Reson.* 64, 255-270 (1985)
- [19] J.L. Prince, J.M. Links, "Medical Imaging Signals and Systems", Pearson Prentice Hall, (2006)

- [20] B.Akin, Y.Eryaman, E.Atalar "A method for phantom conductivity and permittivity measurements", 26<sup>th</sup> Annual ESMRMB Meeting, Antalya, Turkey October 1-3, (2009).
- [21] P. A. Bottomley, A. Kumar, W. A. Edelstein, J. M. Allen, and P. V. Karmarkar, "Designing passive MRI-safe implantable conducting leads with electrodes" *Med. Phys.* 37, 3828 (2010)
- [22] H.Virtanen, J.Huttunen , A.Toropainen and R.Lappalainen "Interaction of mobile phones with superficial passive metallic implants" *Phys. Med. Biol.* 50, 2689-2700 (2005)